

# Structure and Evolution of a Dwarf Galaxy's Circumgalactic Medium

Jacob Vander Vliet<sup>1</sup>, Christopher W. Churchill<sup>1</sup>, Sebastian Trujillo-Gomez<sup>1</sup>,  
Elizabeth Klimek<sup>1</sup>, Anatoly Klypin<sup>1</sup>  
<sup>1</sup>New Mexico State University



astronomy.nmsu.edu/jrvander

## Introduction & Motivation

A major driver of galaxy evolution is how gas flows in and out of the galaxy. Gas infalling from the intergalactic medium mixes with gas outflowing from the interstellar medium in the circumgalactic medium (CGM). The nature of the CGM reflects both the galaxy's accretion star formation history. Due to its tenuous nature, the CGM cannot be observed in emission. The CGM is typically observed using absorption lines in the spectrum of a background quasar. This method has been used for decades by observers. Simulations of galaxy formation can aid in interpreting observations and testing theories of how galaxies evolve over time. Recent cosmological simulations have been able to create realistic galaxies, with stellar properties that match what is observed. Many simulation struggle to create the observed CGM. The simulated CGM is a strict test on the accuracy of the simulation's physics and models. In order to compare the simulations of observations, the simulations must be observed using the same method of observations. Lines of sight are run through the simulated CGM and mock quasar absorption lines are created based on the composition, kinematics, and ionization properties of the gas along the line. These mock lines are then analyzed using the same techniques as for observations.

## The Simulations

The simulations we used are from a cosmological zoom-in simulation suite were run by Sebastian Trujillo-Gomez as described in Trujillo-Gomez et al., 2013. These used a Eulerian Gasdynamics plus N-body Adaptive Refinement Tree (ART) code with descriptions for supernova feedback and radiation pressure. We analyze a single dark matter halo for a present day dwarf galaxy ( $M_{vir} = 3 \times 10^{10} M_{\odot}$ ,  $R_{vir} = 80$  kpc). The halo was re-run to redshift zero using different description of physics to test the effects of radiation pressure. The difference in the runs are shown in Table 1.

Model	Feedback	$\tau_{UV}$	$\tau_{IR}$	$\tau_{tot}$
dwSN	SNI+SW	-	-	-
dwRP_1	SNI+SW+RP	1	0	1
dwRP_8	SNI+SW+RP	1	7	8

**Table 1: Simulation Parameters** SNI+SW indicates supernova and stellar winds, and RP stands for radiation pressure.  $\tau$  stands for the optical depth used in the radiation pressure description for different wavelengths.

We also follow a single physics description (dwRP\_8) before and after a burst of star formation to examine how the CGM is affected by the starburst. To explore the CGM, we post-processed the CGM to determine the ionization conditions of the gas based on the temperature, density, and background radiation field. We focused on the commonly observed ions HI, MgII, CIV, and OVI. These ions trace different phases of gas, from cold ( $10^4$  K) gas traced by HI and MgII, to warm ( $10^5$  K) traced by CIV, to hot ( $10^{5.5}$  K) gas traced by OVI.

## Generating Absorption Spectra

To generate the absorption profile, we ran 1000 lines of sight (LOS) through each simulated box, aligned so the galaxy is face on. The impact parameter and position angle of each line is randomly selected. The maximum impact parameter is  $1.5 R_{vir}$ , corresponding to 120 kpc at redshift zero. The optical depth of each cell that lies along the LOS is added to the absorption profile, depending on the velocity of the cell's gas.

This spectrum is then convolved with the ISF of the appropriate instrument for that transition and redshift, generating realistic spectra. An example is shown in Figure 1. Once the spectra are made, the equivalent width and AOD column density are calculated.

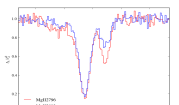


**Figure 1 - Example spectra** This is a sample MgII spectra for dwRP\_8 at redshift zero.

## Phase Diagrams At Present Day

We generated a density-temperature plot for each galaxy we examined. The simulations were each galaxy were cut into two bins at 10% of their virial radius. This cut roughly separates the gas that is inside the galaxy from the CGM. The results are presented in Figure 2. The inner regions are not heavily affected by the different feedback descriptions. However, the addition of radiation pressure changes the CGM into a cooler environment.

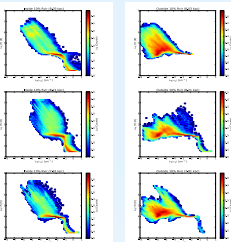


**Figure 2 - Phase diagrams for Different Feedbacks** Each row is a different feedback model. The top row is dwSN, the middle row is dwRP\_1, and the bottom row is dwRP\_8. The left column is only gas within  $0.1 R_{vir}$  and is dominated by the ISM. The right column is the rest of the gas and is dominated by the CGM.

## Covering Fraction

We calculated the covering fraction (CF) profile of the CGM with projected distance from the galaxy by determining the fraction of absorbers with  $W_{\lambda} \geq W_{cut}$  in fixed impact parameter bins. Here, we used  $W_{cut} = 0.0 \text{ \AA}$ , so all absorption is shown. Increasing  $W_{cut}$  would decrease the CF by cutting out the weaker absorbers. The strength of this effect can be estimated from the equivalent width vs. impact parameter plots shown in Figures 6 and 7. In general, the CF decreases with increasing  $D$ . The results for the different feedbacks are shown in Figure 3. These results show that dwRP\_1 creates the most extended CGM for all metal ions. For HI, dwRP\_8 is able to create the biggest halo. dwSN is unable to create a significant metal halo.

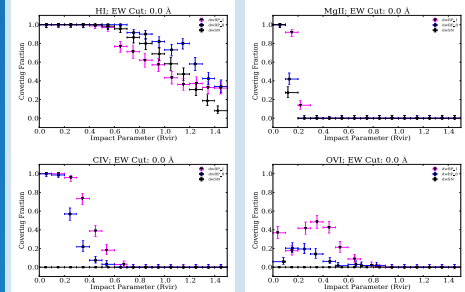


**Figure 3 - Covering Fraction Profiles** The covering fraction profile for different  $D$  bins and ions. Horizontal bars indicate the  $D$  bin width and vertical bars are  $1\sigma$  binomial uncertainties. Points are plotted at the mean  $D$  for each bin. The pink points are for dwRP\_1, the blue points are for dwRP\_8, and black points are for dwSN.

The evolution of the covering fraction during a starburst is shown in Figure 4. Before the star burst, the HI covering fraction builds up slowly while the CIV CF builds up sharply. The MgII CF is initially very steep, but then flattens out during the starburst. The CIV CF drops as well. After the starburst, the MgII and CIV steepens again. The OVI CF is initially very low, but grows greatly right before the starburst. After the burst, the OVI CF fluctuates.

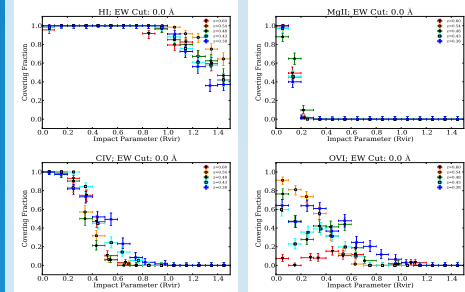


**Figure 4 - Covering Fraction Profiles** The covering fraction profile for different  $D$  bins and ions. The bars are the same as in Figure 3. Points are plotted at the mean  $D$  for each bin. The colors go from red to blue corresponding to redshift.

## Phase Diagram Evolution

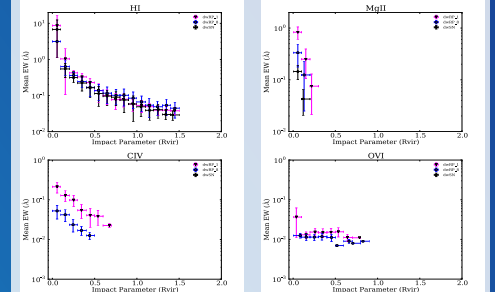
We also examined the phase plots of the simulation dwRP\_8 before and after a starburst, as presented in Figure 5. The galaxy experienced a burst in star formation at  $z=0.5$ . We examined two timesteps before and two timesteps after the burst. The starburst has a distinct effect on the CGM, making it hotter. The starburst causes the inner regions to become hotter and less dense. The outer regions have a distinct cool and dense region before the event, but this gas disappears after the starburst. The gas also creates hot, low density gas to appear in the outer regions.

**Figure 5 - Phase Diagrams for dwRP\_8 During a Starburst** Each row is a different timestep. The top row is  $z=0.60$ , followed by  $z=0.54$ ,  $z=0.48$ ,  $z=0.43$ ,  $z=0.38$ . The left and right columns are as in Figure 4.

## Equivalent Width vs. Impact Parameter

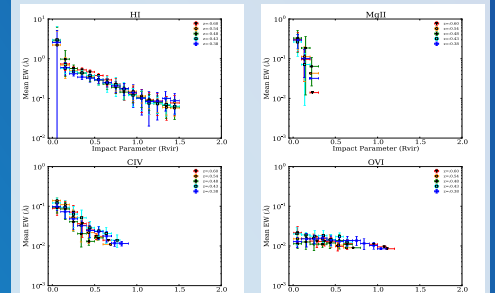
We measured the equivalent width (EW) of each spectrum generated and looked for any trend with impact parameter. To more easily compare across different redshifts, the impact parameter was scaled by the halo's virial radius. There has also been recent results (Churchill et al, 2013a) that indicates the CGM is self-similar when scaled by the virial radius.

Figure 6 shows the results for the four ions at redshift zero for the three different simulations. In general, the observed EW decreases as the impact parameter increases. Hydrogen is found at all impact parameters, while the cool ion, MgII, are only found in close to the galaxy. Warmer ions, like CIV, can be found further out, while the hot ion, OVI, can be found to large impact parameters. The HI distribution is not affected by the differing feedback mechanisms, but the metals are strongly affected. Radiation pressure is required to produce significant metal absorption in the CGM. dwRP\_1 is able to create larger EW than dwRP\_8 due to the lower SF rate caused by the stronger radiation pressure in dwRP\_8. It is important to note that the OVI EW is on average  $0.01 \text{ \AA}$ , below the detection limits of most instruments.



**Figure 6 - Mean Equivalent Width vs. Impact Parameter** The mean equivalent width profile for different  $D$  bins and ions. Horizontal bars indicate the  $D$  bin width and vertical bars are  $1\sigma$  binomial uncertainties. Points are plotted at the mean  $D$  for each bin. The pink points are for dwRP\_1, the blue points are for dwRP\_8, and black points are for dwSN.

We repeated the analysis for the dwRP\_8 star burst event, shown in Figure 7. There is little change in the EW spatial distribution for any ion during this event. The only trend is in OVI, which is most extended well before and well after the event. The event seems to destroy the outer edges of the OVI halo.



**Figure 7 - Mean Equivalent Width vs. Impact Parameter Evolution** The mean equivalent width profile for different  $D$  bins and ions. Horizontal bars indicate the  $D$  bin width and vertical bars are  $1\sigma$  binomial uncertainties. Points are plotted at the mean  $D$  for each bin. The colors go from red to blue corresponding to redshift.

## Summary

**Adding radiation pressure to the feedback:**

- Increases the amount of CGM metals
- Struggles to create significant OVI
- Creates a cooler and denser CGM

**During a starburst:**

- Metal covering fraction increases
- CGM increases in temperature
- EW vs  $D$  does not change significantly

## Future Work

We will continue to analyze the galaxies presented here by looking at the kinematics of the gas and by performing full Voigt profile fits to the synthetic spectra. We will also look at the other galaxies presented in Trujillo-Gomez et al 2013, which includes two additional radiation pressure formulas and a higher mass halo ( $2 \times 10^{11} M_{\odot}$ ). We will add more ions to our list to more effectively probe the different phases, such as NaI, CaII, SiIV, and NeVIII.

## References

Churchill, C. W., Nielsen, N.M., Kerpak, Glenn, C., Trujillo-Gomez, Sebastian, Arzou, Kenza, & Primack, Joel, 2013, arXiv: 1311.2199  
Trujillo-Gomez, Sebastian, Klypin, Anatoly, Collins, Pedro, Coorssen, Daniel,